Electronic Supplementary Material (ESI) for Journal of Materials Chemistry C

Supporting Information

Role of ionic chlorine in the thermal degradation of metal chloride-doped graphene sheets

Ki Chang Kwon[a], *Buem Joon Kim*[b,c], *Jong-Lam Lee*[b,c,*], and *Soo Young Kim*[a,*]

[a] School of Chemical Engineering and Materials Science, Chung-Ang University

221 Heukseok-dong, Dongjak-gu, Seoul 156-756, Republic of Korea

[b] Department of Materials Science and Engineering, Pohang University of Science and Technology (POSTECH), Pohang, Gyeongbuk 790-784, Republic of Korea

[c] Division of Advanced Materials Science, Pohang University of Science and Technology (POSTECH), Pohang, Gyeongbuk 790-784, Republic of Korea

CORRESPONDING AUTHOR FOOTNOTE

*E-mail: jllee@postech.ac.kr, Tel: 82-54-279-2152, Fax:82-54-279-2399

sooyoungkim@cau.ac.kr, Tel: 82-2-820-5875, Fax: 82-2-824-3495

The stability of doped graphene sheets was investigated. (Fig. S1) As air exposure time goes by, sheet resistance of all of the samples slightly increased compared to that of as-doped graphene.

The Raman spectroscopy of as-doped and annealed samples was displayed. (Fig. S2 (a) and (b)) The red dashed line means G band and 2D band peak of pristine graphene sheet. The G band and 2D band of as-doped sample shifted to higher wavenumber, but those of annealed sample shifted to un-doped pristine graphene peak location.

The metal atomic percentage of each metal chloride doped graphene was displayed in bar chart. (Fig. S3(a)-(f)) The as-doped samples consist of four core level spectra of their metal orbitals, for example, Au $4f_{5/2}$, Au^{3+} $4f_{5/2}$, Au $4f_{7/2}$, and Au^{3+} $4f_{7/2}$. All of atomic percentages of ionic metal orbitals decreased by thermal annealing. Furthermore, all of the annealed samples of each core level peaks shifted to lower binding energy. (Fig. 4(a) ~ (f))

The chlorine atom composition of as-doped and annealed samples also were showed in bar chart. (Fig. S4) The atomic percentage of chlorine atoms of each doped graphene was decreased by thermal annealing process which is agree with decrease in XPS peak intensity of chlorine atom. (Fig. 5) After thermal annealing, atomic percentage of chlorine atoms dramatically decreased to less than 3 %. These results coincide with the XPS data of chlorine peak intensity. (Fig. 5)

In order to verify our proposed mechanism and graphene surface change, the as-doped graphene and thermally annealed samples were measured by SEM images at different magnification levels. (Fig. S5, S6) The number of metal particle was increased by thermal annealing, and these results coincide with decrease of each metal ion peak in XPS data. The higher thermal annealing temperature generates the more aggregated particles which are induced by thermal annealing.

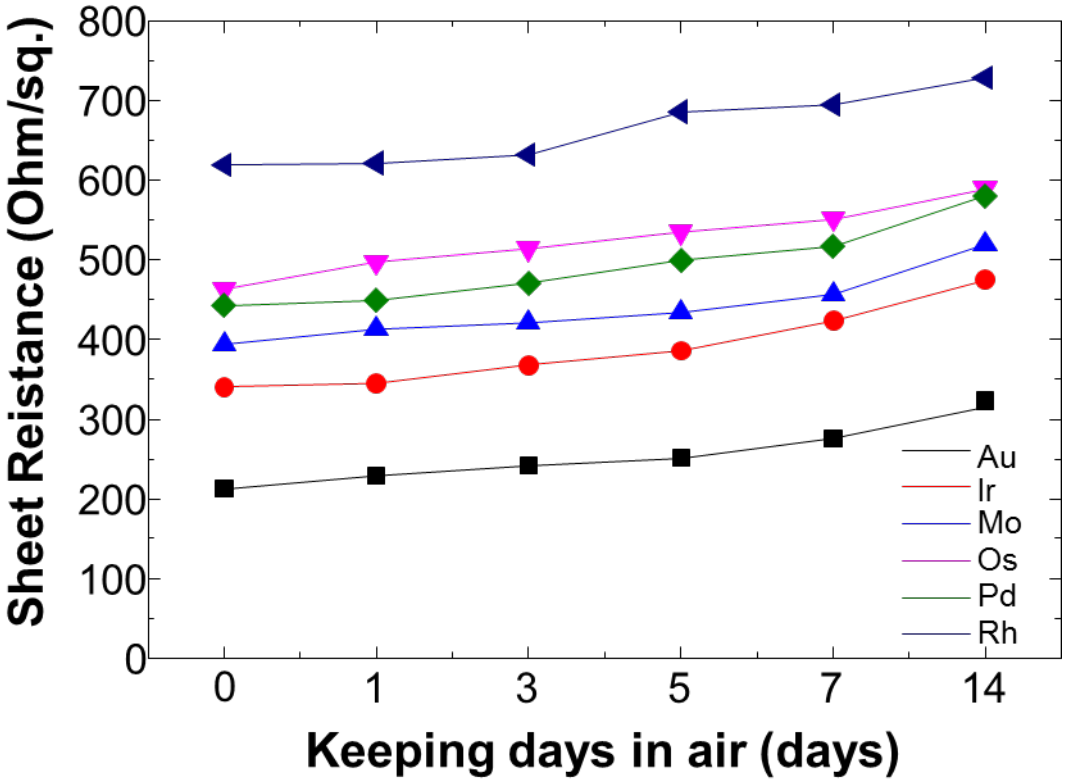

Figure S1. The sheet resistance result as-doped graphene as a function of time for 14 days.

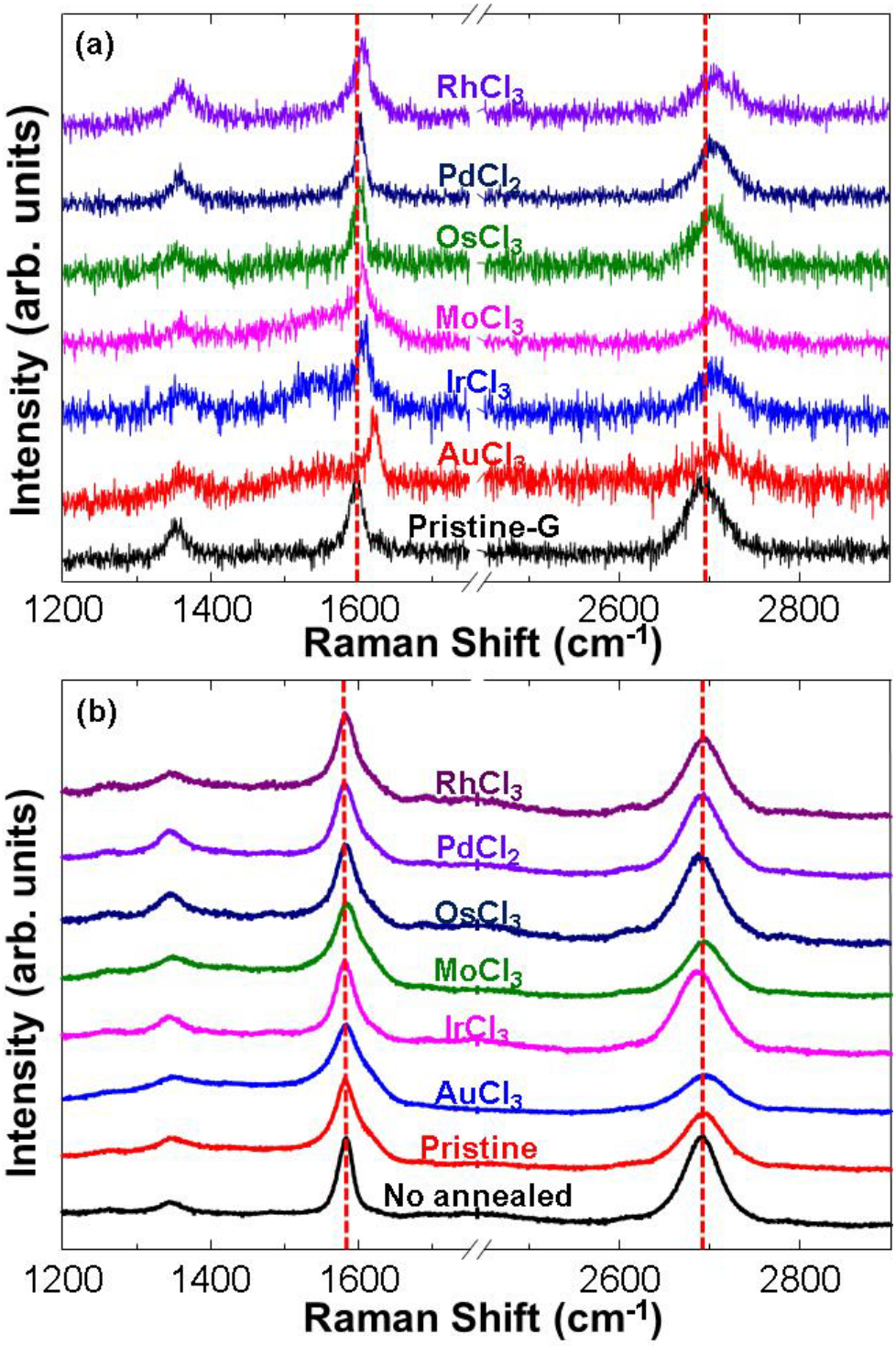

Figure S2. The Raman spectroscopy of (a) as-doped and (b) annealed graphene sheets.

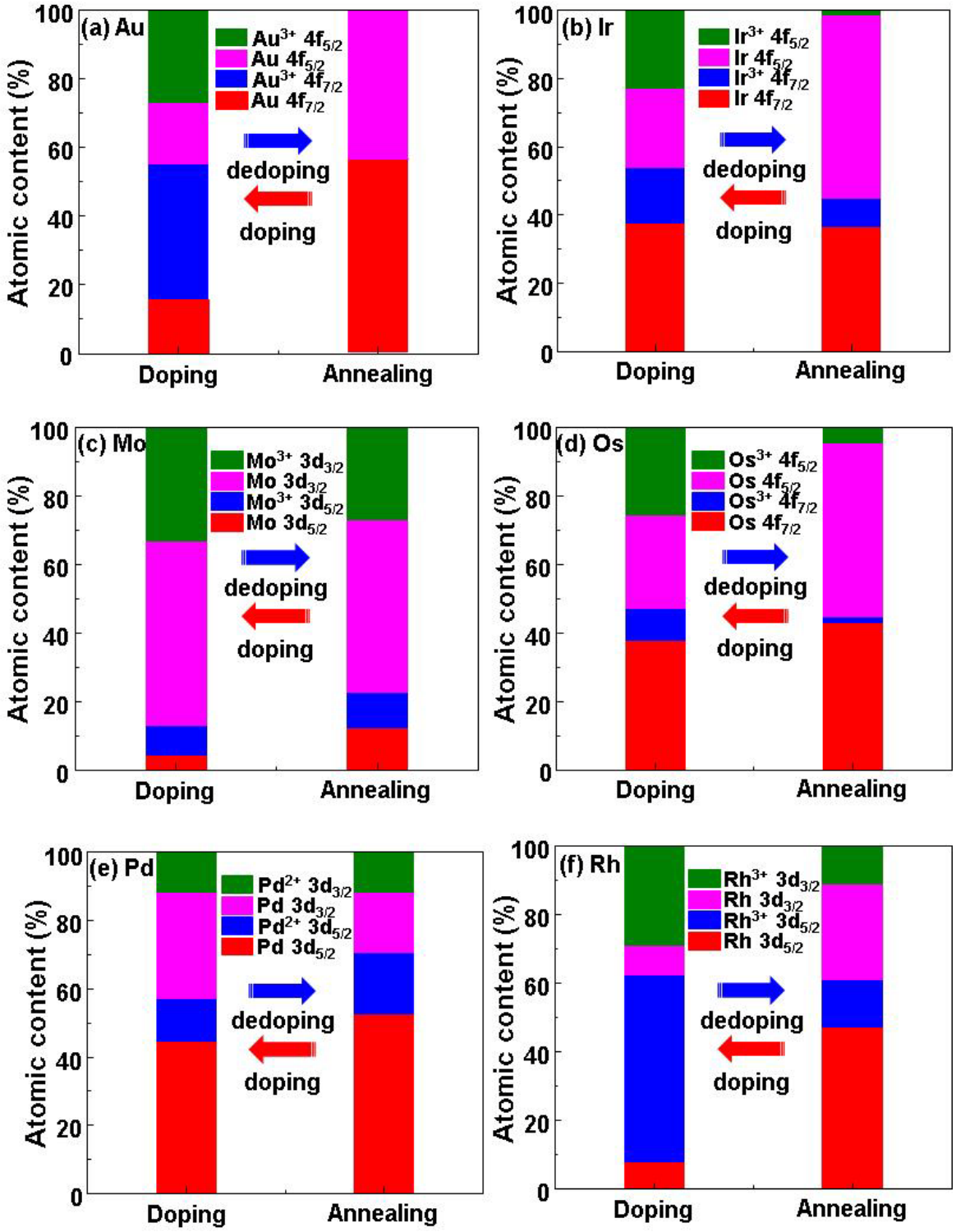

Figure S3. The atomic orbital percentages of each metal XPS peak. (a) $AuCl_3$-doped graphene, (b) $IrCl_3$-doped graphene, (c) $MoCl_3$-doped graphene, (d) $OsCl_3$-doped graphene, (e) $PdCl_2$-doped graphene, and (f) $RhCl_3$-doped graphene.

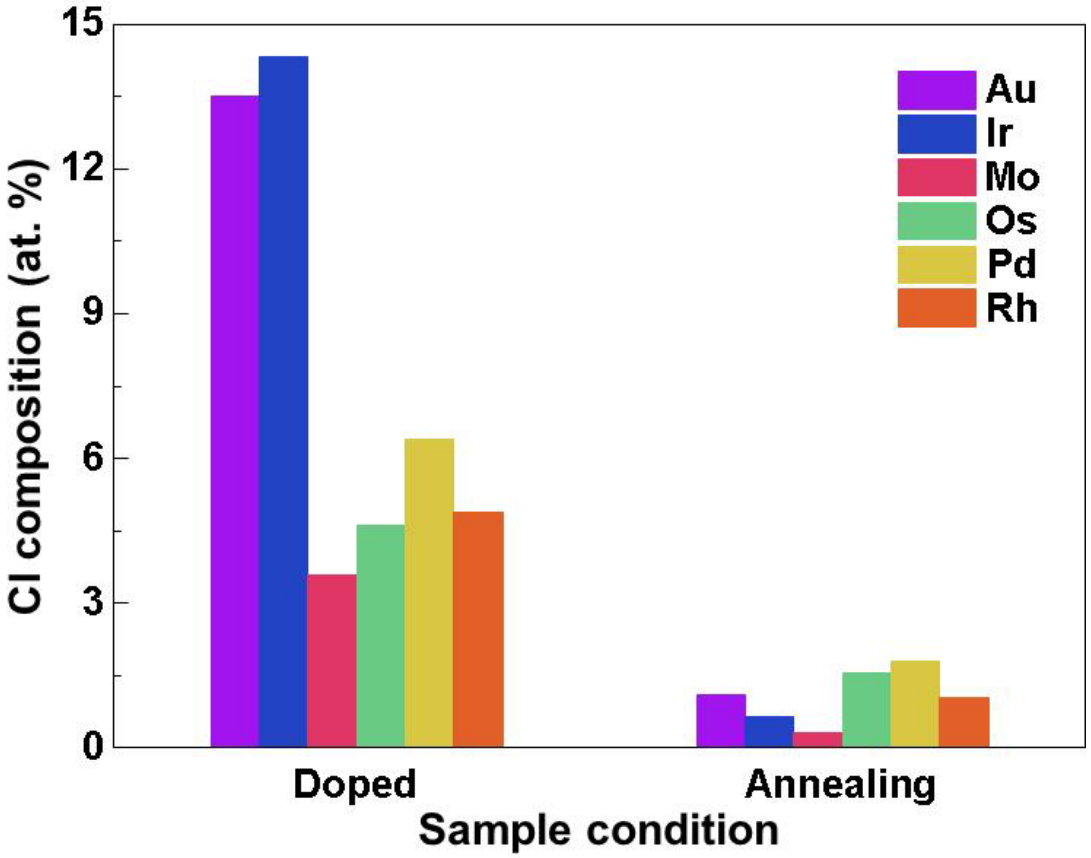

Figure S4. The chlorine atom composition data of each doped graphene XPS peak.

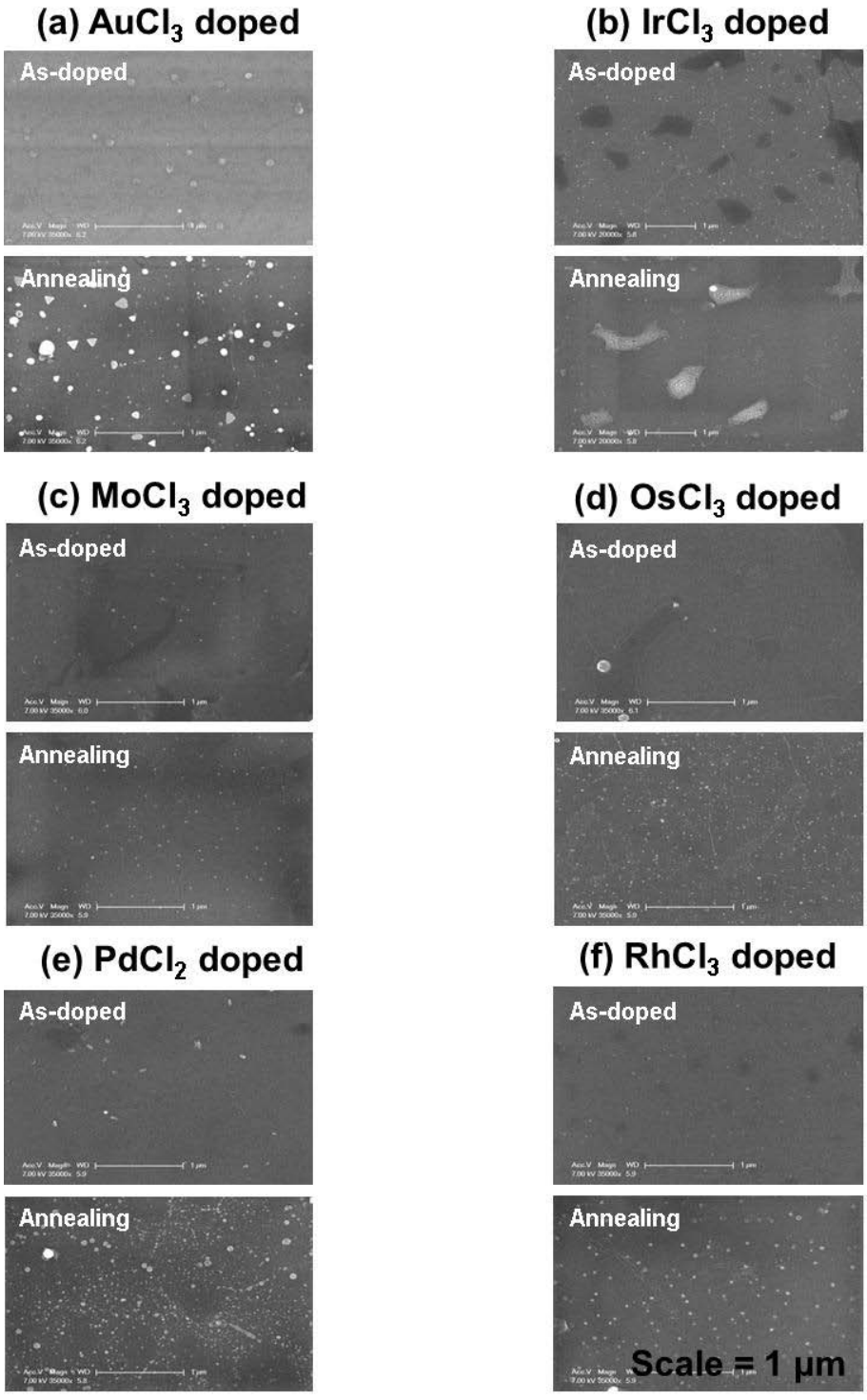

Figure S5. The SEM images of doped and annealed graphene sheet. The scale bar is 1 μm. (a) $AuCl_3$-doped graphene, (b) $IrCl_3$-doped graphene, (c) $MoCl_3$-doped graphene, (d) $OsCl_3$-doped graphene, (e) $PdCl_2$-doped graphene, and (f) $RhCl_3$-doped graphene.

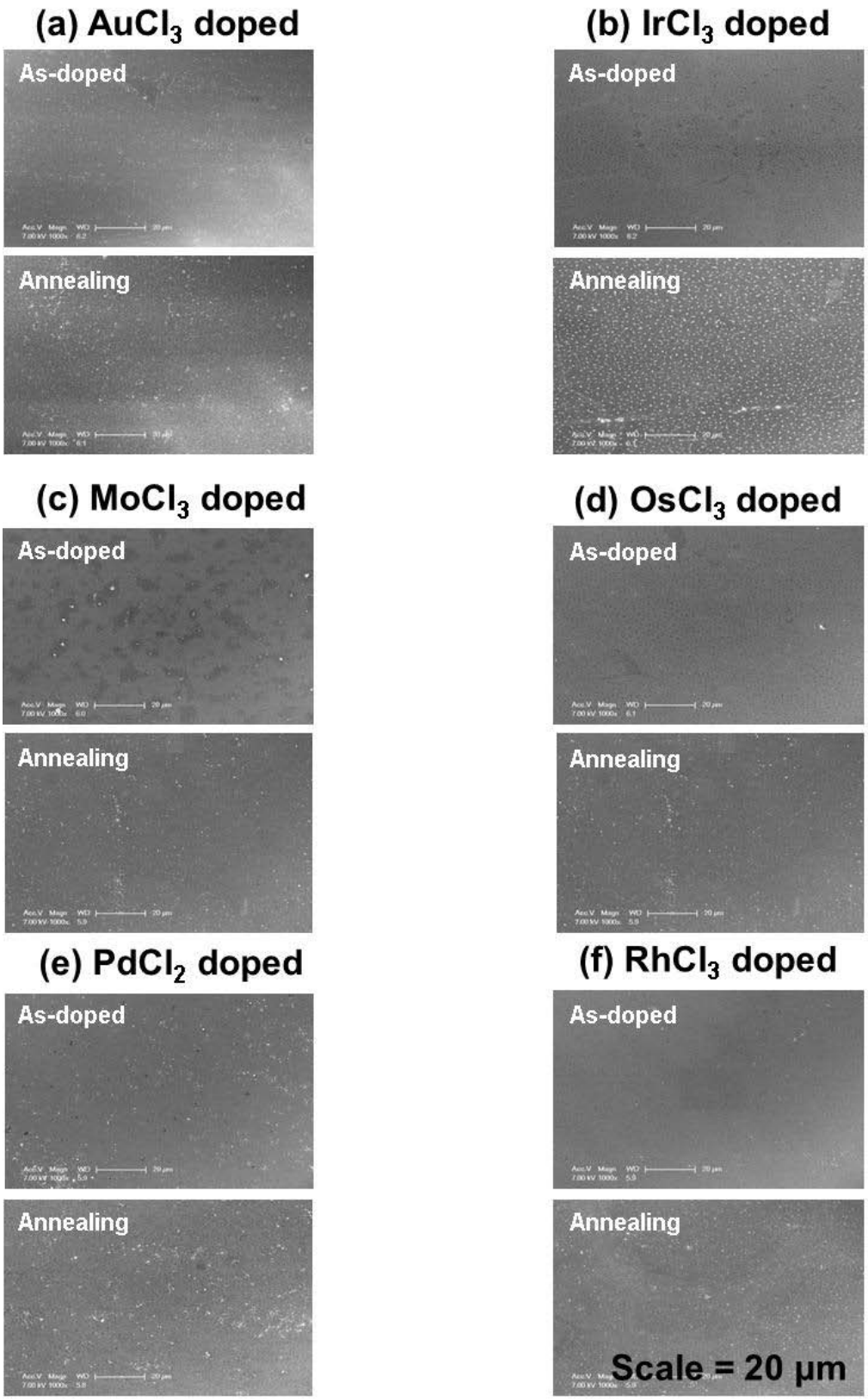

Figure S6. The SEM images of doped and annealed graphene sheet. The scale bar is 20 μm. (a) $AuCl_3$-doped graphene, (b) $IrCl_3$-doped graphene, (c) $MoCl_3$-doped graphene, (d) $OsCl_3$-doped graphene, (e) $PdCl_2$-doped graphene, and (f) $RhCl_3$-doped graphene.